

Fig. 2. The simulator output matched to the AM 1.5 reference spectrum is shown. The addition of 50 nm of coverage over a previous simulator implementation is a significant improvement.

illustrated in Fig. 1 has been described previously [7]. In this instance, a 6 watt super-continuum laser with a spectrum spanning from below 400 nm to beyond 2200 nm was used. The lower limit below 400 nm represents a significant bandwidth increase of more than 50 nm beyond previous demonstrations, extending into an energetic region of the solar spectrum.

The spectrum below 950 nm was controlled by a grating light valve spatial light modulator (GLV-SLM), which is a linear array device with 1088 pixels that operates as a steerable diffraction grating [8]. Spectral components incident on the GLV from a prism made of Schott F2 glass [9] were attenuated by steering them out of the dispersed beam. The desired spectrum was then reflected back through the prism and exited the short wavelength spectral shaper. The spectrum above 950 nm was controlled by a liquid crystal on silicon spatial light modulator (LCOS-SLM) comprised of a

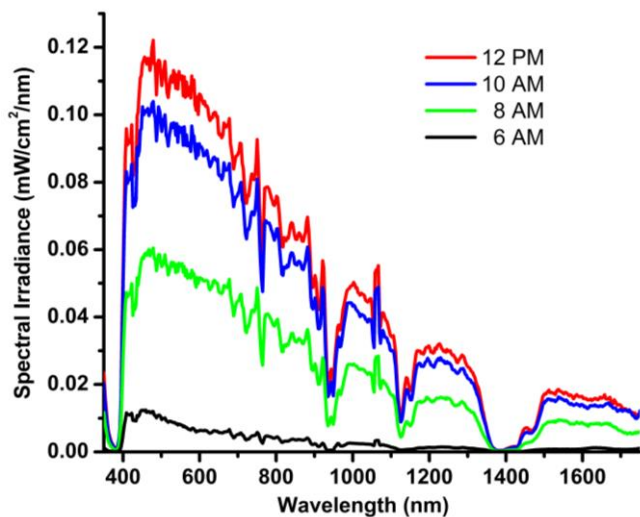


Fig. 3. Selected measurements of the simulator output are shown for the spectral variation of time of day based on SMARTS.

512×512 array of pixels, which was operated as a polarization diversity switch. As shown, the incident light passed through a polarization beam splitter (PBS) before being dispersed by a prism made of Schott SF10 glass [9]. The LCOS-SLM selectively rotates the polarization state of the reflected spectrum, such that it reflects off the PBS and out of the long wavelength spectral shaper.

Light from the two prism spectrometers was then recombined in a multimode fiber with a 200 μm core. Accurate spectral shaping was achieved with an iterative loop between the voltage patterns driving the SLMs and a scanning spectrometer measuring the simulator output from the optical fiber.

Figure 2 presents spectral shaping of our simulator to match the AM 1.5 (ASTM G-173-03) solar reference spectrum [10], resulting in a concentrated irradiance of 100 suns. The 50 nm increase in spectral coverage reduces the mismatch remaining between 300 nm and 400 nm to less than 5 % of the total integrated irradiance. The spectral resolution of the shaping was sufficient to replicate all but the sharpest spectral features, with the highest resolution of ~ 1 nm achieved at short wavelengths. Finite amplitude extinction limited the ability to attenuate the sharp feature at 1064 nm caused by laser pump light. Figure 3 shows selected output spectra as the simulator mimicked the sun during the time of day based on the Simple Model of the Atmospheric Radiative Transfer of Sunshine (SMARTS) [5]. Similar sets of spectra were generated for seasonal and air-mass variations.

Figure 4 illustrates two setups for illuminating a small-area MJ-CPV concentrator cell. In the direct divergent setup, no additional optics are required and the tip of the simulator output fiber was brought to within 2 to 3 mm of the solar cell being measured. This approach takes advantage of the inherent spatial confinement of the optical fiber, which in this setup had an inner core diameter of 200 μm with a numerical aperture of 0.22. The spectrum incident on the cell can be estimated from the scanning spectrometer measurement of the output optical fiber. This estimate assumes that the beam diverges uniformly with wavelength, when in fact long wavelengths will diverge

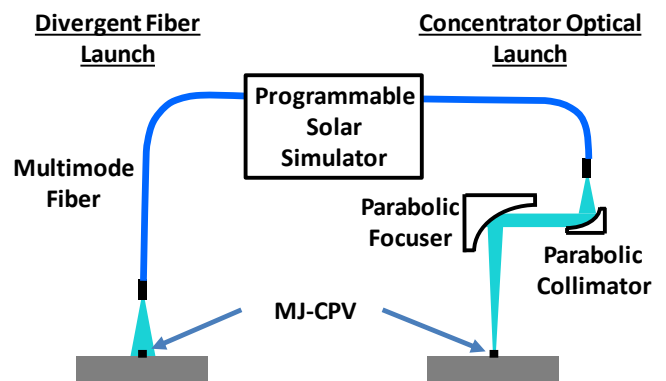


Fig. 4. The two experimental setups used to illuminate an MJ-CPV cell, consisting of a divergent beam with no additional optics and a focused beam created by parabolic mirrors.

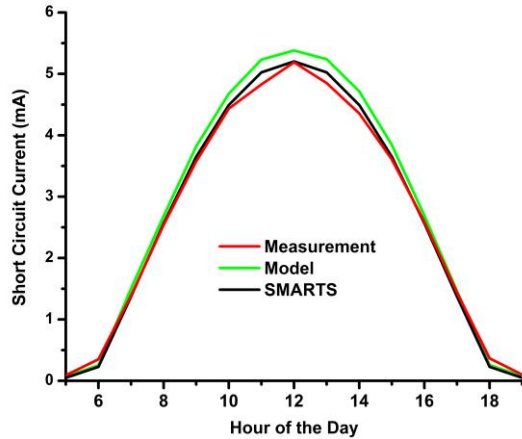


Fig. 5. The measured output of a MJ-CPV cell in response to simulated hour-of-the-day variations is shown for concentrated illumination. Predictions based on measured spectra (Model) and ideal spectra (SMARTS) are included.

more than short wavelengths. The irradiance on the cell is difficult to estimate because of the beam divergence and the uncertainty in the distance between the fiber tip and the cell. In the concentrated setup, the simulator light was collimated and focused with broadband parabolic mirrors. The relatively long focal length of the focusing mirror ($f = 152$ mm) resulted in a soft focus with a large beam waist of 1 mm. By definition, the light is collimated at the waist, where the incident optical power could be measured through an aperture of known size. However, in order for the spectrum incident on the cell to be known, spectral losses associated with the concentrator optics had to be accounted for in advance. Clearly, each of these setups has advantages and disadvantages for the quantitative testing of solar cells.

III. MEASUREMENTS WITH FOCUSED ILLUMINATION

We used the simulator to generate time-of-day spectra representing every hour from 5 AM and 7 PM, similar to the example curves in Fig. 3. Figure 5 shows the measured short circuit current of an MJ-CPV solar cell chip that was fully illuminated by the concentrated beam shown on the right side of Fig. 4. The square solar cell had an active area of approximately $600 \mu\text{m} \times 600 \mu\text{m}$. The concentrated irradiance on the cell was approximately 100 suns. As expected, the current peaked in the middle of the day at 12 PM. Using characteristic quantum efficiency curves for the solar cell, currents were calculated based on measured spectra (labeled “Model”) as well as ideal spectra (labeled “SMARTS”). The model curve lies above the SMARTS curve because the limited resolution of the spectral shaping tended to generate higher average irradiance in regions with substantial fine structure. The agreement between model and measurement is

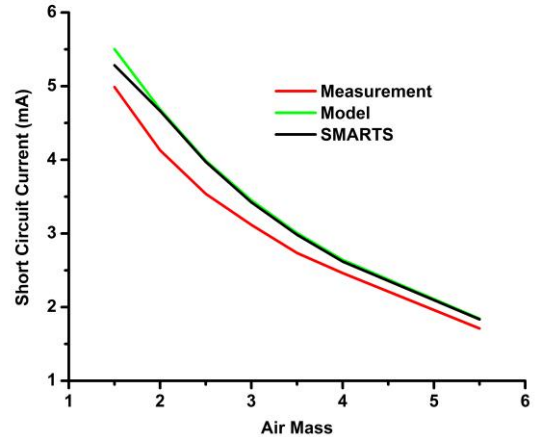


Fig. 6. The measured output of a MJ-CPV cell in response to simulated air mass variations is shown for concentrated illumination. Predictions based on measured spectra (Model) and ideal spectra (SMARTS) are also shown.

dependent on the accuracy of the quantum efficiency curves, calibration of the spectrometer relative to the concentrated beam power, equipment dynamic range, and compensation for spectral losses. Because the simulated spectra were measured at the multimode fiber output, spectral compensation for the collimator and focusing mirror, and correction for the finite area of the solar cell was required. The agreement would likely improve significantly if the incident spectrum could be measured directly. Overall, the agreement in Fig. 5 is quite good at better than 10 %, and indicates that the simulator can realistically mimic the sun based on SMARTS spectra

Figure 6 shows the decrease in measured short circuit current from the MJ-CPV in response to simulated light for

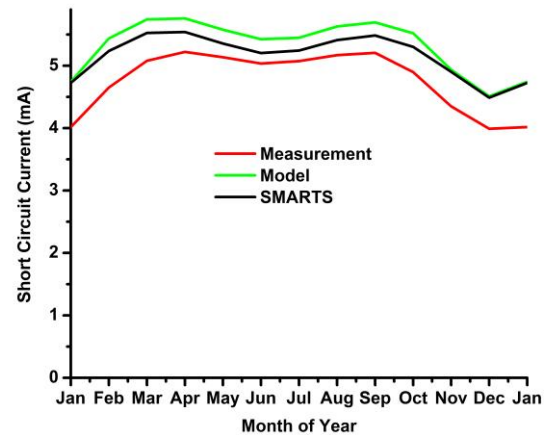


Fig. 7. The measured output of a MJ-CPV cell in response to simulated seasonal variations is shown for concentrated illumination. Predictions based on measured spectra (Model) and ideal spectra (SMARTS) are included for comparison.

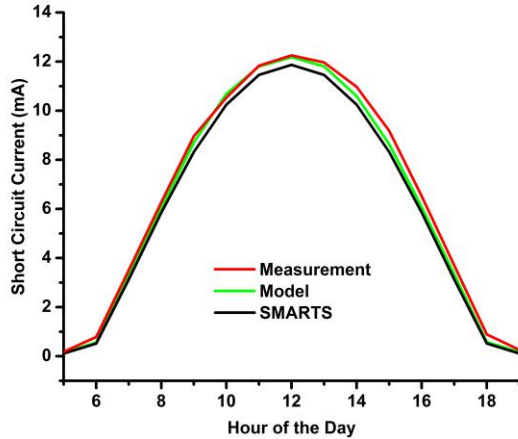


Fig. 8. The measured output of a MJ-CPV cell in response to simulated hour-of-the-day variations is shown for direct divergent illumination. Predictions based on measured spectra (Model) and ideal spectra (SMARTS) are included.

increasing air-mass. Similar to the time-of-day curves, the measurement and model agree to 10 % or better. At an air-mass of 1.5, the difference between model and SMARTS is on par with Fig. 5, but becomes negligible at higher values. This is caused by a transition from the total current being limited by one junction of the cell to another junction of the cell, combined with a reduction in spectral shaping error.

In Fig. 6 the measured seasonal performance of the MJ-CPV is presented for illumination by the concentrated beam. A characteristic double peak in the current production is apparent, with maxima occurring during the spring and fall seasons. During the winter months, the model and SMARTS

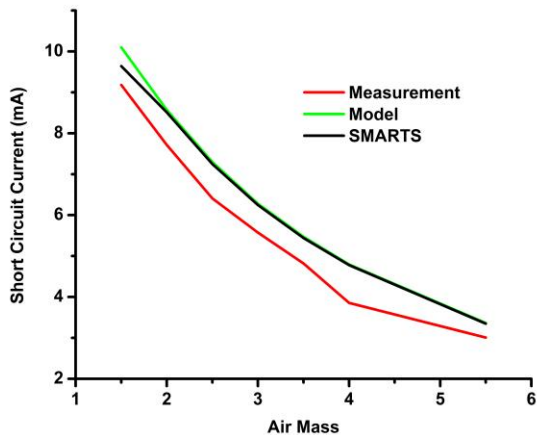


Fig. 9. The measured output of a MJ-CPV cell in response to simulated air mass variations is shown for direct divergent illumination. Predictions based on measured spectra (Model) and ideal spectra (SMARTS) are also shown.

curves agree almost exactly. However, the model curve is consistently higher during the spring, summer, and fall seasons as the junction limiting the total cell current is influenced by more spectral shaping error from finite resolution. Both of the predicted curves are consistently above the measured curve, which is attributed to uncertainty between the measured spectra and the actual irradiance delivered to the cell surface. If it is assumed that 10 % less total optical power was delivered to the cell, then both the model and SMARTS curves shift down to better overlap with the measured curve.

IV. MEASUREMENTS WITH DIVERGENT ILLUMINATION

Using the direct divergent illumination setup shown on the left side of Fig. 4, we measured the response of the same MJ-CPV cell as above. Figure 8 shows the measured short circuit current of the cell in response to hour-of-the-day variations, where the effective irradiance on the cell was approximately 190 suns. The measurements agree very well with calculated results based on a model of the multi-junction cell using both measured spectra (labeled “Model”) as well as ideal spectra (labeled “SMARTS”). As mentioned previously, it is difficult to accurately determine the total optical power incident on the solar cell surface with divergent light. Therefore, a scaling factor for the measured spectra used in the model calculations was selected which gave good visual agreement for the curves of short circuit current. Once determined, this same scaling factor was used in all subsequent measurements with divergent light. However, irrespective of this scaling factor, the functional agreement or shape of the curves matches very well, indicating again that the simulator can realistically mimic the sun based on SMARTS spectra.

Figure 9 shows the decrease in measured short circuit

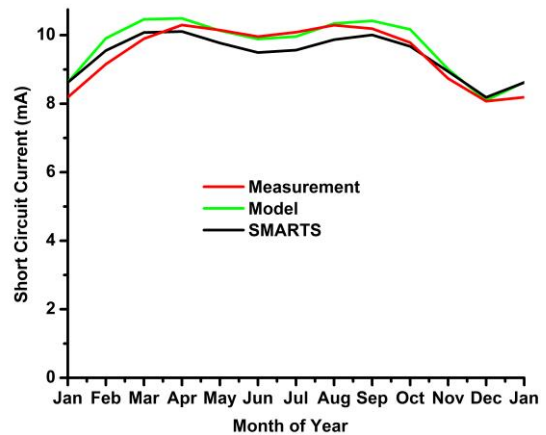


Fig. 10. The measured output of a MJ-CPV cell in response to simulated seasonal variations is shown for direct divergent illumination. Predictions based on measured spectra (Model) and ideal spectra (SMARTS) are included for comparison.

current from the MJ-CPV for increasing air-mass with direct divergent illumination. As compared to the concentrated illumination results above, the difference between the measurement and model curves is generally somewhat larger, and may indicate that the spectral scaling factor had drifted slightly. It is also worth noting that the average short circuit current is about twice as large as the concentrated illumination measurement.

The dependence of the MJ-CPV short circuit current on the month of the year is shown in Fig. 10 for direct divergent illumination. While the average agreement between the measured and model curves is very good and a consequence of the spectral scaling factor, the shapes differ some. The measured dependence has less of a pronounced dip in current in the middle of the summer. While the exact cause has not been determined, it may be the result of current limiting or luminescent coupling between the junctions that is not captured by our simplistic model. This same behavior was also observed in the concentrated illumination measurements of Fig. 7.

V. DISCUSSION AND CONCLUSION

By use of a super-continuum laser with an additional 50 nm of spectral coverage down to 400 nm, we were able to reduce the theoretical limit for spectral mismatch from 11 % down to less than 5 %. This limit assumes that the spectral shaping process has sufficiently high resolution so as not to introduce spectral mismatch of its own. In a multi-junction cell, the impact of the remaining mismatch of 5 % depends on which junction is responsible for limiting the total cell current. In this work, the remaining lack of light between 300 and 400 nm had less impact on measurements than not knowing exactly what light was being delivered to the cell surface. Super-continuum lasers are now available which extend down to 350 nm and below; however, they tend to produce low optical power.

We expect that the observed differences between our measurements and predictions of short circuit current could be significantly reduced with a more sophisticated method of measuring the spectrum and total optical power delivered to the cell surface. Our demonstration of two different cell illumination geometries illustrated some of the challenges. For the focused illumination, it was possible to know fairly accurately the power delivered to the cell surface, yet difficult to know the exact shape of the spectrum. The required spectral correction factors can potentially vary slightly with time as well as beam alignment. In the case of the direct divergent illumination, it was possible to know the spectrum incident on the cell fairly well, but difficult to estimate the irradiance over the active area of the cell. For this geometry, better measurement agreement may also be obtained by quantifying the beam divergence as a function of wavelength. One solution for measuring the spectrum and optical power delivered to the cell may be to use an area-matched aperture in place of the

solar cell followed by an integrating sphere for spatial uniformity.

It may seem counterintuitive that the divergent illumination resulted in a higher concentration of irradiance than the focused one; however, this is simply a consequence of the optics, losses, and working distances selected. The direct divergent illumination makes use of the spatial confinement of the 200 μm optical fiber core. With a numerical aperture of 0.22, the emitted light expands to a 1 mm diameter at a distance of 2.2 mm. For focused illumination, a measured spot size of 1 mm was achieved with a parabolic objective having a focal length of 152 mm. The loss and broadband compensation for the spectral dependence of the parabolic mirrors limits the total amount of light that can be delivered to the focused spot. A smaller spot would increase the concentration but result in less uniform illumination.

The novel super-continuum solar simulator has been shown to be a sophisticated tool for the characterization of the complex operation of solar cells such as multi-junctions at high concentration. With commercial laser systems on the horizon offering substantial increases in optical power, we anticipate that an even wider range of measurement conditions will become available to the solar cell researcher.

REFERENCES

- [1] K. Emery, D. Myers, and S. Rummel, "Solar simulation – problems and solutions", in *Twentieth PVSC*, Las Vegas, NV, pp. 1087-1091, 1988.
- [2] C. H. Seager, "The determination of grain-boundary recombination rates by scanned spot excitation methods," *J. Appl. Phys.*, vol. 53, no. 8, pp. 5968-5871, 1982.
- [3] B. H. Hamadani, J. Roller, B. Dougherty, and H. Yoon, "Fast and reliable spectral response measurements of PV cells using light emitting diodes," in *Thirty-ninth PVSC*, Tampa, FL, 2013.
- [4] S. R. Kurtz, K. Emery, and J. M. Olson, "Methods for analysis of two-junction, two-terminal photovoltaic devices," in *Proc. World Conf. Photovoltaic Energy Convers.*, Waikoloa, HI, USA, pp. 1733-1737, 1994.
- [5] C. Gueymard, "Parameterized Transmittance Model for Direct Beam and Circumsolar Spectral Irradiance," *Solar Energy*, 71:5, pp. 325-346, 2001.
- [6] T. Dennis, J. B. Schlager, and K. A. Bertness, "A Novel Solar Simulator Based on a Super-Continuum Laser for Solar Cell Device and Materials Characterization," *IEEE J. Photovoltaics*, vol. 4, no. 4, pp. 1119-1127, 2014.
- [7] T. Dennis, B. Fisher, M. Meitl, and J. Wilson, "A High-Concentration Programmable Solar Simulator for Testing Multi-Junction Concentrator Photovoltaics," in *Forty-second PVSC*, New Orleans, LA, 2015.
- [8] D. T. Amm and R. W. Corrigan, "Optical Performance of the Grating Light Valve Technology," in *Proc. SPIE 3634, Projection Displays V*, pp. 71-78, 1999.
- [9] Product names are only used in the paper for clarity and do not represent an endorsement by NIST.
- [10] Standard Tables for Reference Solar Spectral Irradiances: Direct Normal and Hemispherical on 37° Tilted Surfaces, G173003, 2008. Available: <http://astm.org>